Heliyon 9 (2023) e21992

Contents lists available at ScienceDirect

Heliyon

journal homepage: www.cell.com/heliyon

Enhanced O_2/N_2 separation by QuaternizedMatrimid/Multiwalled carbon nanotube mixed-matrix membrane

Mallikarjunagouda Patil [a,**], Savitri G. Hunasikai [a], Shridhar N. Mathad [b], Arun Y. Patil [c], Chandrashekhar G. Hegde [d], M.A. Sudeept [d], M.K. Amshumali [e], Abdallah M. Elgorban [f], Shifa Wang [g], Ling Shing Wong [h], Asad Syed [i,*]

[a] Bharat Ratna Prof. CNR Rao Research Centre, P. G. Department of Chemistry, Basaveshwar Science College, Bagalkot 587101, India
[b] Department of Engineering Physics, K.L.E Institute of Technology, Hubballi 580030, India
[c] Department of Mechanical Engineering, Manipal Institute of Technology Bengaluru, Manipal Academy of Higher Education, Manipal, Karnataka, India-576104
[d] School of Mechanical Engineering, KLE Technological University, Vidya Nagar, Hubballi 580031, India
[e] Department of Industrial Chemistry, Vijayanagara Sri Krishnadevaraya University, Ballari 583105, India
[f] Centre of Excellence in Biotechnology Research, King Saud University, Riyadh, Saudi Arabia
[g] School of Electronic and Information Engineering, Chongqing Three Gorges University, Wanzhou, 404000, China
[h] Faculty of Health and Life Sciences, INTI International University, Putra Nilai, 71800 Nilai, Negeri Sembilan, Malaysia
[i] Department of Botany and Microbiology, College of Science, King Saud University, P.O. 2455, Riyadh, 11451, Saudi Arabia

ARTICLE INFO

Keywords:
Matrimid
MWCNT
O_2/N_2 selectivity
Membrane
Separation

ABSTRACT

The air separation (O_2/N_2) based on polymeric membranes is critical because it is more energy efficient than traditional methods. Dense polymeric membranes are now the main stay of industrial processes that generate oxygen and nitrogen enriched gas. Though, regular polymeric membranes often fall short of selective pressure demands because O_2 and N_2 gases have such comparable equivalent diameters. While polymer composites have their benefits, nanocomposite (NCs) allows for the production of high-performance barriers. Utilising Matrimid® 5218 (Matrimid) as the base framework and multiwall carbon nanotube (MWCNT) as the filler, a novel NCs for O_2/N_2 separation was developed. Both matrimid and MWCNTs were chemically modified quaternization and functionalizing the MWCNTs. The membranes were casted using solution casting with a combination of quaternized matrimid and functionalized multi-walled carbon nanotubes (*f*-MWCNT). When *f*-MWCNT was added to quaternized matrimid, it created interfacial compatibility, which increased O_2/N_2 selectivity and permeability by 65 % and 35 %, respectively. In the current study, increasing O_2 diffusivity and O_2/N_2 solubility selectivity resulted in improved performance, this paves a way for manufacturing innovation.

1. Introduction

More than half of the energy consumed in the chemical manufacturing sector is spent on the separation of liquid or gaseous substances [1]. Chemical separation and purification in refinery and petroleum product processes use a lot of energy, such as low

* Corresponding author.
** Corresponding author.
E-mail addresses: mallupatil04@gmail.com (M. Patil), assyed@ksu.edu.sa (A. Syed).

https://doi.org/10.1016/j.heliyon.2023.e21992
Received 25 May 2023; Received in revised form 25 October 2023; Accepted 1 November 2023
Available online 8 November 2023

temperature olefin/paraffin mixture distillation or extractive distillation in the manufacture of benzene and the isomeric compounds of xylene separation via low temperature fractional crystallization. The basic cost of chemicals such as ethylene, toluene, benzene, and propylene could be significantly decreased if the separation technique could be improved. Membrane separation technology will open up new avenues for separating gaseous and liquid mixtures. Membrane distillation units are much smaller than traditional distillation units, and the operation can be performed at lower temperatures. In some cases, a hybrid process combining distillation and membrane units has been established. Membrane distillation units are much smaller than traditional distillation units, and the operation can be performed with lesser temperatures. In some cases, a hybrid process combining distillation and membrane separation units has been established. According to estimates, membrane-based hybrid processes will save 40–50 % of production costs in the separation of olefin/paraffin binary mixtures [2].

The separation of O_2 and N_2 gaseous components has piqued the interest of non-technical industries such as the chemical and medical industries [1]. In fuel combustion processes, for example, the use of oxygen-enriched air is typically recommended because a higher oxygen concentration in oxidant gas ensures increased total energy efficiency [2,3]. Furthermore, oxygen-enriched air has been shown to improve the efficacy of sewage treatment plants [4]. Further, highly pure nitrogen is used to extend the shelf life of food, in coal extraction (as a fire extinguisher during the mining operation) [5] in wet chemical laboratories (synthesis) and chemical transportation [6–8], and in the storing of cryogenics that utilizes liquid nitrogen [9–12].

Air separation technology has long used pressure-swing adsorption (PSA) and cryogenic distillation techniques. The truth is that these technologies can generate large amounts of high-purity gases, but a significant impediment with respect to increased energy demand and capital expenditure [13,14] is expected. Because of its simplicity and low cost, membrane-based gas separation has recently piqued the interest of academics. Polymer-based membranes are frequently used in gas separation methods, but the solution-diffusion process that regulates gas movement in such membranes causes a trade-off between permeability and selectivity [15,16]. Because of their low scalability, plain molecular sieve-based membranes are currently not easily deployable in commercial applications [17]. As a result, it has been recognised that there is a theoretically feasible opportunity for producing scalable membranes with high-performance qualities by developing new generation mixed-matrix membrane (MMM) that syndicates the benefits obtained in combination of polymeric membranes and zeolites, inorganic fillers or molecular sieves [18,19].

The fillers or additives used in gas separation membranes can have a big impact on their performance and efficiency. Fillers are commonly employed to improve the selectivity and permeability of membrane materials, allowing for improved gas separation capabilities. Several factors influence the filler material selection, including the target gases to be separated, the membrane matrix material, and the required performance criteria. Inorganic or organic fillers include zeolites, metal-organic frameworks (MOFs), carbon nanotubes, graphene, and polymer nanoparticles. It should be noted that the filler selection and concentration should be carefully tuned to obtain the desired gas separation performance. The qualities of the fillers, their compatibility with the membrane matrix, and the general shape of the membrane all play important roles in determining the efficacy of the filler selection. Because of their small effective kinetic diameters of 2.89 Å for O_2 and 3.04 Å for N_2 [20,21], efficient divergence of O_2 and N_2 from the air has become difficult. Because of the small diameter difference, molecular sieving (via porous materials as fillers such as zeolites, clay or MOFs) cannot be used as the individual driving force of separation. Furthermore, because N_2 adsorption is more polarizable than O_2 adsorption, i.e., O_2: 17.4×10^{-25} cm^3 vs. N_2: 15.8×10^{-25} cm^3 [22], most adsorbents prefer N_2 adsorption over O_2 adsorption. Despite this, numerous metal-organic frameworks (MOFs) with high O_2/N_2 selectivity exist, including the chromium (II) carboxylate MOF (Cr_3BTC_2) and MOF-5. However, as the number of working cycles increases, the structural instability of the system limits its practical utility [23–25]. In contrast, polymers with inherent microporosity (PIMs) have demonstrated excellent O_2/N_2 separation performance [26–28]. PIMs are not immune to polymer ageing, which causes a progressive decline in membrane function over time [29–32]. In this case, aided carriers (in the form of molecules and solid particles) open up exciting new possibilities for developing next-generation O_2/N_2 separation membranes.

The enabled carriers that penetrate one of the gas molecules in gas mixture are preferred by the bounding process. While N_2 is inactive, the hopping process occurs during the selective and reversible complexation of O_2 via transport events [33]. Cobalt-based complexes such as cobalt (II) phthalocyanine (CoPC), cobalt (II) tetraphenylporphyrin (CoTPP), and cobalt (III) acetylacetonate (Co (acac)3) stand out for their O_2 selectivity among the carrier alternatives for facilitating O_2 transport [33–37].

Matrimid® 5218's permeability must be increased before it can be used to construct a high-performance nanocomposite membrane. As described in the literature [38]. Non-selective voids, on the other hand, can cause larger defects to form, resulting in a significant decrease in selectivity performance [39]. To overcome this problem, multiwalled carbon nanotube particles must be compatible with base polymer matrices. Surface modification of carbon nanotube particle particles, such as with *tert*-butyl groups, is one possible approach [34,38]. A subsequent chemical modification process, on the other hand, is frequently required. Many groups [40,41] have found that block copolymers can be effective compatibilizers between fillers and polymer matrices.

We provide a high-performance O_2/N_2 separation nanocomposite membrane made of multiwall carbon nanotube particles embedded in Matrimid® 5218. (Matrimid). According to gas permeation research, adding 5 % multiwall carbon nanotube particle improves the permeability of O_2 and O_2/N_2 selectivity by 68 % and 35 %, respectively. The Matrimid multiwall carbon nanotube particle system outperformed the clean polymer in both O_2 diffusivity and O_2/N_2 selectivity, according to a study of solubility/diffusivity (Matrimid). Given that each constituent of the Matrimid multiwall carbon nanotube particle system is widely available and reasonably priced, the nanocomposite architecture demonstrated here appears to have large-scale membrane fabrication potential.

2. Materials and methods

2.1. Materials

Chemicals supplied by Fine Chemicals, Mumbai, included chloroform, methanol, ethanol, sulfuric acid, triethylamine (TEA), and concentrated paraformaldehyde. Concentration of hydrochloric acid, cyclohexane, and zinc chloride. Because each sample was of sufficient quality for analysis, it was used as is. Sigma Aldrich manufactured MWCNT. The PTFE adhesive was created by Sigma-Aldrich (USA). Activated carbon and the Vulcan XC-72 (20 % platinum in carbon support) were provided by WonatechPrivate Limited, respectively. Cabot Carbon Inc. Provided the carbon fabric. To make cathode catalysts, our lab synthesised 10 % Ag and 1 % Pd–Ni on Vulcan XC-72. The DMAMFC's anode and cathode materials were obtained from WonatechPvt. Ltd. In India. Only double-distilled water was used in the preparation of all solutions. The chemical structures of (a) MWCNT and (**b**) Matrimid® are displayed in Fig. 1.

2.2. Synthesis of anion exchange membrane

The chemical processes of chloromethylation and quaternization were used in the generation of anion exchange membranes. The procedure for experimenting with an ionomer was described in the scientific literature [24,25], and the results were thoroughly examined. We did not describe the steps that led us to choose matrimid over polystyrene ethylene butylene polystyrene (PSEBS).

2.3. Functionalization of MWCNTs

MWCNTs will be ultrasonically treated with a 3:1 ratio of sulfuric acid and nitric acid to incorporate carboxylic acid groups onto their surface. After mixing everything together, the acid was removed by washing it with cold distilled water and centrifuging it until the pH of the supernatant reached 7, indicating that the suspension was no longer acidic. The prepared material was dried for 6 h in a vacuum oven at 100 °C.

2.4. Preparation of composite membrane

A solution of dissolved matrimid in cyclohexane was mixed with various amounts of *f*-MWCNTs for approximately 24 h. To achieve the required membrane thickness, the solution was ultrasonically treated for about 15 min before being spread on a clean Petri dish and dried at 50 °C for 8 h. Because MWCNTs are expensive, two weight ratios of MWCNT-embedded matrimid membranes (5 and 10 % wt.%) were created and studied. The results were compared to a matrimid membrane devoid of MWCNTs. Table 1 contains instructions for preparing the membranes.

2.5. FTIR

FTIR was used to investigate the chemical composition and interactions between polymers and inorganic fillers. By keeping the membranes in KBr windows and operating the spectrometer in transmission mode, we were able to obtain FTIR spectra for the matrimid and other composite membranes.

2.6. UV–visible spectroscopy

A spectrometer (Systronics, Bangalore) was used to perform the UV–visible analysis at a scanning speed of 100 nm min^{-1}.

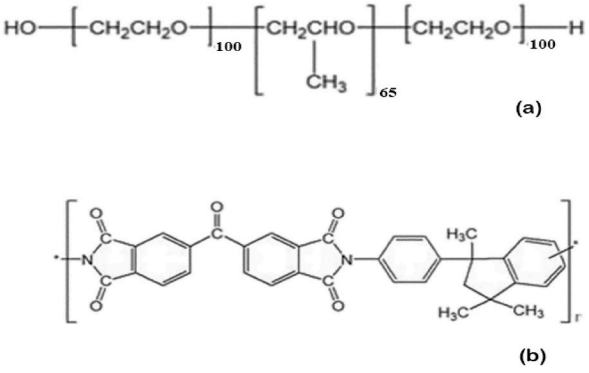

Fig. 1. Chemical structures of (a) MWCNT and (**b**) Matrimid®.

Table 1
Membrane composition and nomenclature.

Sl. No	Matrimid (gm)	*f*-MWCNT (gm)	Wt. %of *f*-MWCNT	Name
1	4	0	0	M@*f*-MWCNT_0
2	4	0.2	5	M@*f*-MWCNT_5
3	4	0.4	10	M@*f*-MWCNT_10

2.7. XRD analysis

Powder XRD tests on membrane samples were measuredusing powder X-ray diffractometer (Make: Siemens Model: D 5000) having CuKα source and a scanning rate of 0.5° sec^{-1}. The generated output signals from XRD as curves were analysed and indexed using the Proszki software package, and the results of the powder XRD research are consistent with those of the single crystal XRD.

2.8. Thermogravimetric analysis

In the study, TGA systems (Brand: TA Instruments, Model: Q500) were used. For the measurements, the prepared samples were heated from room temperature to 700 °C at a rate of 4 °C min^{-1} in N_2 atmosphere at a flow rate of 25 mL min^{-1}.

2.9. Mechanical properties

The tensile strength and percentage of elongation of the fabricated composite membranes were tested using universal testing equipment (Make: Hounsfield). To reproduce the results, membrane samples were cut into 5 mm by 50-mm pieces [29]. Despite a force of 50 N applied to it, the crosshead maintained a speed of 10 mm min^{-1}. A minimum of three separate measurements were obtained for each test, and the average of these was used.

2.9.1. Scanning electron microscopy (SEM)

The M@*f*-MWCNTs subsequently disseminated in ethanol for microscopy specimen preparation, and the several droplets of the dispersion were placed on a fresh clean silicon wafer platform. The annealed membranes were fractured in liquid nitrogen to check the cross-sectional images of the test specimens, accompanied by gold sputtering onto Matrimid and its functionalized MWCNT composite membranes to provide high-quality SEM images. The morphology was examined using a JEOL SEM, model JSM-7600F.

2.10. EDAX

We confirmed the dispersibility of f-MWCNTs in the NMMM using energy-dispersive X-ray spectroscopy (EDAX, JSM-7600F, JEOL, Akishima, Tokyo, Japan), resulting in the best potential performance of the membrane (from the gas permeation test).

2.11. Porosity

To determine the porosity and gas adsorption profile of M@*f*-MWCNTs, a volumetric gas sorption analyser and N_2 physisorption at 77 K were used (Quantachrome, LX2, USA). Before testing, the samples were outgassed for 6 h at a temperature of 413.15 K to remove any impurities and remaining solvent.

2.12. Raman spectroscopy

The Raman R3000 system and an 8-mm, 509-nm working-length objective were used to obtain the spectra. He–Ar lasers were used on the sample to generate an excitation wavelength of 532 nm with a surface power of 0–90 mW and a spot size of approximately 3 lm. The matrimid and other composite membranes were placed in a quartz in-situ Raman sample cell.

2.13. Cyclic voltammetry (CV) studies

The CV tests were carried out with a three-electrode setup and a Wonatech model WPG100ex potentiostat/galvanostat instrument. The active electrode was a glassy carbon electrode (GCE) with a surface area of 0.0707 cm^2. Platinum wire and an extremely saturate calomel electrode used as the working and reference electrodes, respectively (SCE). The SCE reference electrode was used to plot all potentials in this analysis. The potential window was −1.0 to 1.0 V, and the scan rate was 25 mV s^{-1}.

2.14. Gas adsorption analysis

The volumetric gas sorption analyser was used to evaluate the membranes' pure O_2 and N_2 adsorption isotherms at 308.15 K. and pressures ranging from 0 to 5 bars (iSorb HP1, Quantachrome, Boynton Beach, FL, USA). Gas adsorption (q) was calculated with each membrane by extrapolating the O_2 and N_2 isotherm models, taking into account that the isotherm is linear across the measurement

range of interest (0.21 bar for O_2 and 0.79 bar for N_2). The following established relationship i.e., equation (1) is used to evaluate gas solubilization in the membrane, (e.g., O_2 and N_2) [6,42].:

$$S = \frac{q\rho}{p} \tag{1}$$

where 'q' denotes the amount of gas adsorbed per mass of membrane, 'p' the pressure, and is the membrane density. This calculation assumes no competing O_2 and N_2 adsorption in the membrane [7,37,43]. D, or gas diffusivity in the membrane, is calculated by dividing permeability by solubility.

2.14.1. 16Gas permeability test of O_2/N_2

To mount the membrane, a stainless-steel male and female coupling membrane holder was used. A constant pressure-variable volume configuration was used for the gas permeation testing. Helium (He) and compressed air (O_2/N_2: 21/79, O_2 99.8 %, and N_2 99.999 %). The membrane was first placed in a heated permeation cell set to 35 °C. A back pressure regulator was installed on the feed side to regulate the feed side pressure while keeping the permeate side pressure constant for atmospheric pressure. Temperature and applied feed pressure were measured across the membranes for O_2 and N_2 gas. Automated gas chromatography (Agilent, Model: 990 Micro GC Systems) with a thermal conductivity detector and a Hysep-Q capillary column was used to analyse the gaseous streams on the permeate and retentate sides. The temperature of the detector was maintained at 523 K, while the injector port and oven were held at 423 K.

Permeance, P_i (mol/m^2 s Pa) of component gas *i* was computed by using equation (2).

$$P_i = \frac{J_i}{\Delta p_i} \tag{2}$$

Ji represents the flux of constituent "i" (mol/m^2 s), "p_i" represents the partial pressure difference across the zeolite membrane (p_a), and "i" may represent O_2 or N_2.

The membranes' selectivity was calculated by employing formula, the ratio of single O_2 andN_2 permeances.

3. Results and discussion

3.1. Functionalization of MWCNTs

Before carbon nanotubes (CNTs) can be widely used as reinforcements in polymer composites, two major challenges must be overcome [31]. The fundamental issue is that CNTs tend to aggregate into packets, resulting in a poor interfacial connection between the CNTs and the polymer matrix, which reduces the composites' electrical and mechanical properties [32]. Improving load transfer efficiency through the formation of a strong interface between the composite (fillers) and polymer is critical to resolving this problem. Surface functionalization of carbon nanotubes is a common method for accomplishing this [33,34]. In general, functionalization results in surface defects in carbon nanotubes, altering the degree of conjugation and reducing charge carrier mobility [35].MWCNTs are less prone to aggregation than SWCNTs, and their conductivity is not significantly reduced because only the surface layers can be

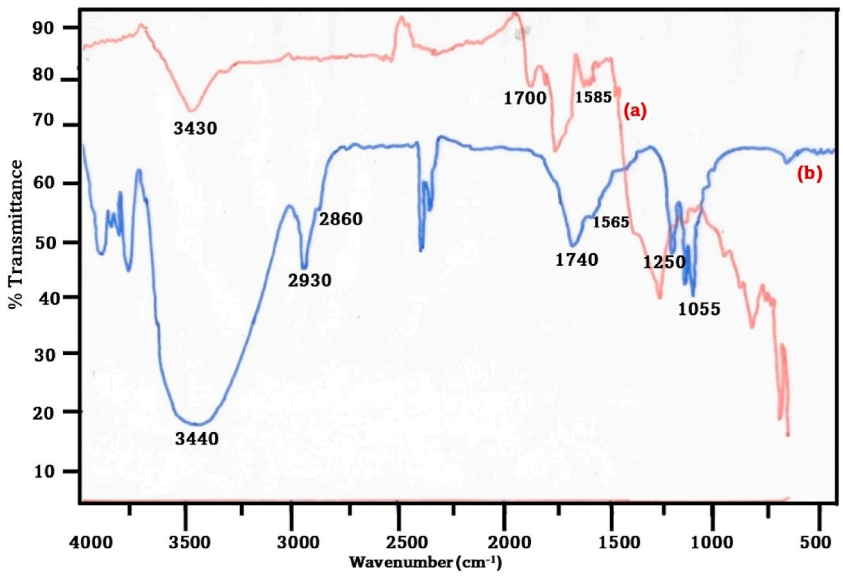

Fig. 2. FTIR spectra of (a) MWCNT and (b) *f*-MWCNT.

functionalized [36]. Furthermore, MWCNTs are less likely to be capable of storing electrons.

3.2. FTIR

According to FT-IR analysis, carbon nanotubes contain carboxylic acid groups. Fig. 2 depicts the FTIR spectra of MWCNT and *f*-MWCNT. The FTIR spectra of MWCNT reveal four main peaks at 3430, 1700, and 1585 cm^{-1} which was displayed in Fig. 2 (a). The O–H stretch from carboxyl groups (O]C–OH and C–OH) is responsible for the peak at 3430 cm^{-1}. The C]O stretching mode of carboxylic acids is responsible for the peak at 1700 cm^{-1}. The peak at 1585 cm^{-1} corresponds to the C]C stretching mode, which emanates from the MWCNT backbone. Furthermore, the peak at 1050 cm^{-1} is attributed to the C–O stretching vibration. The absorption peaks in Fig. 2 (b) are located at 1568, 2930, 2860, and 3440 cm^{-1} (b). The hydroxyl group is represented in the spectral data by a band at around 3440 cm^{-1} (–OH). The widths of the bands produced by asymmetric and symmetric C–H stretching were approximately 2930 and 2860 cm^{-1}, respectively. The peaks at 1740 and 1220 cm^{-1} represent carboxylic acid group stretching, respectively, while the peak at 1565 cm^{-1}corresponds to the infrared-active phonon mode of the *f*-MWCNTs. These findings unequivocally demonstrate the occurrence of –COOH moiety on the surface of *f*-MWCNTs.

3.3. UV–visible spectroscopy

The results of an analysis of the UV–visible spectra of M@*f*-MWCNT_10 and matrimiddispersal in cyclohexane solvent are shown in Fig. 3 to determine how the MWCNTs interact with the quaternized polymer matrix. UV–visible spectroscopy was used to measure the colloidal stability of M@*f*-MWCNT_10 dispersions [38], and dispersion behaviour was investigated in relation to solubility parameters based on filler and polymer interactions [39]. The nanocomposite absorbed more than the bare polymer at 260 nm, indicating that M@f-MWCNT_10 andmatrimid interact primarily via bonding [40,41].

The bonding interaction between Matrimid, a type of polyimide polymer Fig. 3(a) and multi-walled carbon nanotubes (MWCNTs) can vary with increasing absorbance [44]. However, it's important to note that the term "absorbance" typically refers to the ability of a material to absorb light, usually in the context of spectroscopy. The relationship between absorbance and the bonding interaction between MWCNTs and Matrimid might not be direct.

The UV–Visible spectral curve of M@*f*-MWCNT_10 was depected in Fig. 3(b). When MWCNTs and Matrimid come into contact, several types of interactions can contribute to their bonding: (i) van der Waals forces: MWCNTs possess a high aspect ratio and a large surface area, which allows them to interact with the Matrimid through van der Waals forces. These forces arise from temporary fluctuations in electron density and can lead to attractive interactions between the nanotubes and the polymer chains. (ii) π-π stacking: MWCNTs are composed of carbon atoms arranged in a hexagonal lattice, creating a network of delocalized π electrons. Similarly, polymeric materials like Matrimid can have conjugated aromatic structures. These aromatic rings can undergo π-π stacking interactions with the graphene-like structure of the MWCNTs. This stacking interaction can further enhance the bonding between the nanotubes and the polymer. (iii) Electrostatic interactions: Matrimid can contain charged functional groups that can interact with the charged surface of MWCNTs. These electrostatic interactions can contribute to the bonding between the two materials. (iv) When absorbance increases, it implies that more light is being absorbed by the material. However, it's not immediately clear how this relates to the bonding interaction between MWCNTs and Matrimid. The absorbance of a material is typically influenced by its chemical composition, structure, and optical properties. It may not directly correlate with the bonding interactions between the nanotubes and the polymer.

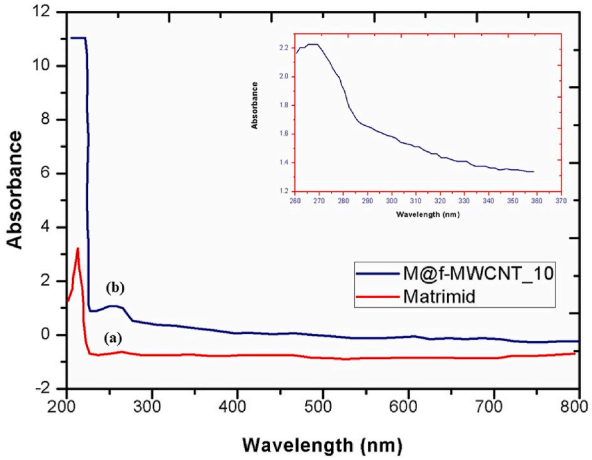

Fig. 3. UV–Visible spectra of (a) Matrimid and (b) M@*f*-MWCNT_10 %; Inset: Expanded view of (b).

3.4. TGA

The thermal stability of matrimid composite membranes was examined using TGA in a N_2 environment. Fig. 4 depicts the thermogravimetric curve of a developing matrimid membrane (a). Between 50 and 550° Celsius, the mass decreases threefold. The first phase occurred at temperatures lower than 100 °C and coincided with water evaporation. The desorption of bound water and the disintegration of quaternary ammonium groups could have caused the second loss, which occurred at around 150° Celsius. The third weight loss at around 450 °C indicates the start of polymer backbone decomposition (i.e., decomposition of carbon chains and phenyl groups, respectively). Fig. 4(b) depicts virgin *f*-MWCNT composites and Fig. 4(c) depicts M@*f*-MWCNT-10 composites. MWCNT incorporated to the polymer matrix synergistically improved the thermal stability of composite membranes. The composite membrane's mass decreased slightly. MWCNT integration determines the mechanical stability of composite membranes in this way.

3.5. Mechanical properties

Because superior mechanical properties of polymer nanocomposites are required for the gas separation and the gas pressure withstand efficiency [42], they are commonly integrated into a polymer matrix. The tensile strength of matrimid and its composite membranes was tested under fully hydrated conditions. With tensile values of 70.2 MPa for the M@*f*-MWCNT_10 and 60.3 MPa for the M@*f*-MWCNT_5, the composite membrane outperforms the nascent matrimid membrane by 219 % and 187 %, respectively (32.11 MPa). Interfacial bonding and features between fillers and polymer matrix are well known to affect the mechanical properties and structural integrity of composite materials [43]. The increased mechanical strength [45] measured by nanoindentation indicates that the modified MWCNTs are distributed uniformly throughout the matrimid membrane matrix with minimal aggregation.

3.5.1. Field emission scanning electron microscopy study (FESEM)

The surface morphology of the developing matrimid membrane was examined using FESEM, and a composite membrane was prepared. Fig. 5 shows SEM images of matrimid membranes and matrimid membranes implanted with MWCNTs. The surfaces of the Matrimid (Fig. 5(a)) and M@*f*-MWCNT_5 composite membrane (Fig. 5(b)) were both smooth and uniform, according to SEM analysis. MWCNTs were found to be evenly distributed throughout the quaternized polymer matrix. Photos of the MWCNTs/matrimid membranes region revealed white patches when cyclohexane was embedded in oxidised MWCNTs using the solution cast method, indicating that the multiwalled carbon nanotubes could be successfully embedded. The establishment of covalent bond or ionic bond between the carbon nanotubes and the matrimid is most likely responsible for the improved dispersion. Fig. 6 shows a SEM image of the M@f-MWCNT_5 in cross-section. The prepared membranes are uniform and have an average thickness of 53 μm, as shown in the image.

3.6. EDAX

Fig. 7 depicts the EDAX spectra and FE-SEM images of commercially available MWCNT and *f*-MWCNT. Large bundles of micron-scale MWCNTs with diameters ranging from 10 to 20 nm were discovered. After oxidation and ultrasonic treatment, the f-MWCNTs were shorter and rougher, and acid treatment disentangled them. The presence of other elements in the corresponding EDAX spectra confirmed their presence.

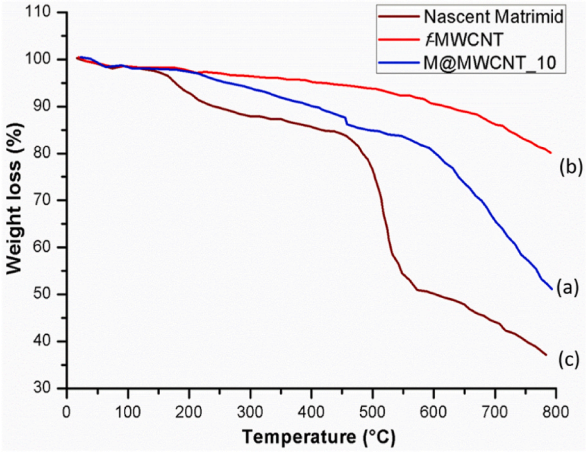

Fig. 4. TGA curves of nascent matrimid membrane, *f*-MWCNT and M@*f*-MWCNT_10.

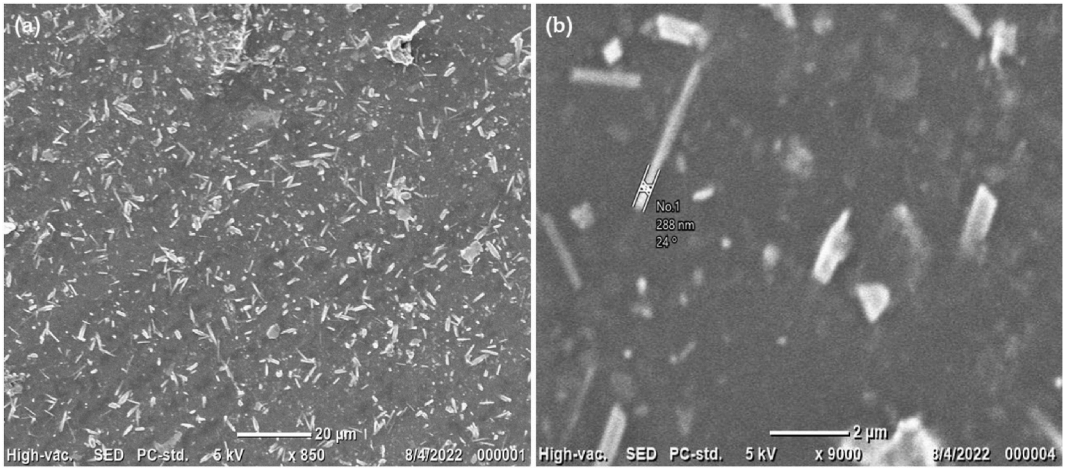

Fig. 5. SEM images of (a) M@*f*-MWCNT_5 at 20 µm and (b) M@*f*-MWCNT_5 at 2 µm.

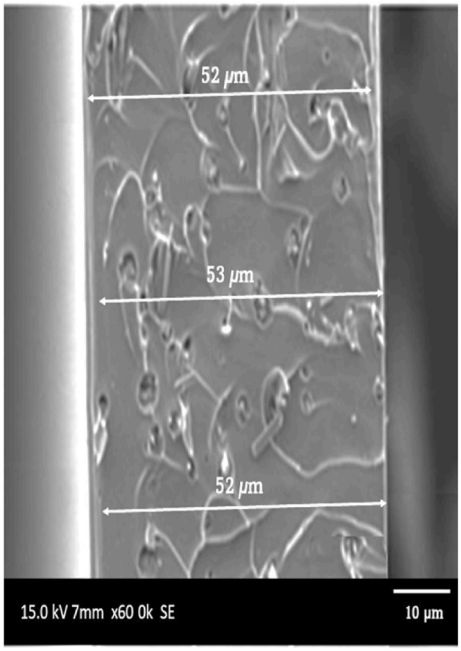

Fig. 6. The M@*f*-MWCNT 5 as depicted in the cross-sectional view of SEM image.

3.7. N_2 adsorption and porosity properties

Fig. 8 and Table 2 shows the N_2 adsorption and porosity properties of the material.

3.8. Raman spectroscopy

Raman spectroscopy has been widely used to evaluate the interaction of polymers and carbon nanotubes in composites [46]. Raman shifts of distinct peaks [47–51] show the interaction between MWCNTs and matrix. Fig. 9(a) shows several prominent peaks in the developing matrimid membrane at 998, 1027, 1190, 1303, and 1440 cm^{-1}. The peak at 998 cm^{-1} is caused by C–N stretching, while the peak at 1303 cm^{-1} is possibly caused by C–H deformation. This shows that the matrimid polymer was quaternized with triethylamine. The G-band (1580 cm^{-1}) and the D-band (1090 cm^{-1}) were the most prominent bands in the Raman spectra of MWCNTs in the composite membrane, as shown in Fig. 9(b) (1340 cm^{-1}). Gas separation applications are feasible due to the efficient incorporation of MWCNTs into the matrimid membrane matrix and the elimination of other characterization peaks present in the naked membrane.

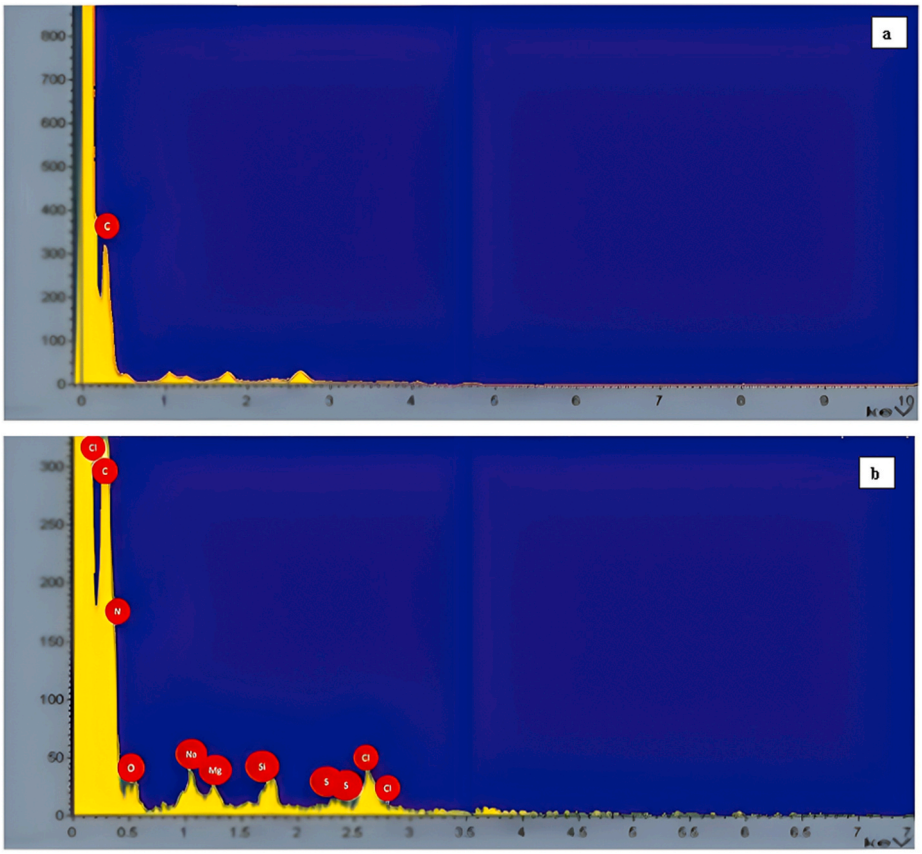

Fig. 7. EDAX spectrumcorresponding to (a) MWCNT, (b) *f*-MWCNT.

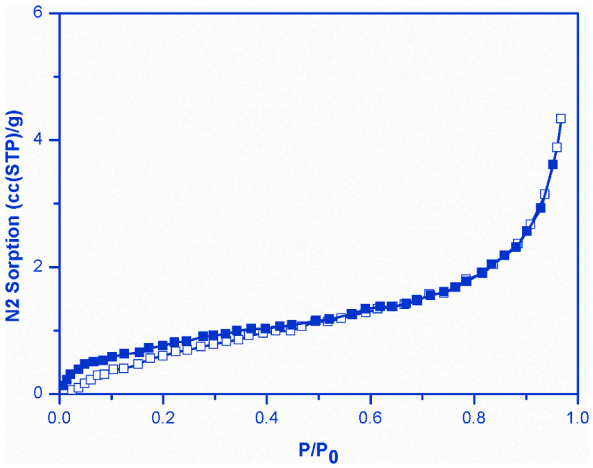

Fig. 8. N2 sorption for *f*-MWCNT at 77 K.

3.9. Cyclic voltammetry studies

Cyclic voltammograms were recorded at the bare GCE, matrimid/GCE, and M@*f*-MWCNT 10/GCE in the presence of 0.5 M KOH and 1 M methanol over potential ranges of −1.0 to +1.0 V (vs. Nonetheless, the quaternized polymer exhibited excellent redox peaks at +0.37 and −0.41 V in a 0.5 M KOH solution, shedding light on the electrocatalytic behaviour of ma.The CVs changed dramatically when the identical reference electrode was immersed in a solution of 0.5 M KOH as well as 1 M methanol.The obtained results were plotted in Figs. 10 and 11.

Table 2
Porosity properties of *f*-MWCNT.

Sample	S_{BET}[a]	$S_{Langmuir}$[a]	V_{micro}[b]	S_{ext}[b]	V_{total}[c]
f-MWCNT	3.11	4.37	0	2.99	0.067

[a] SBET and SLangmuirare calculated by selecting P/Po range from 0.05 to 0.20.
[b] Vmicroand Sext are calculated using *t*-plot method, with P/Po ranging from 0.40 to 0.60 isselected.
[c] Vtotalis calculated at P/Po = 0.99.

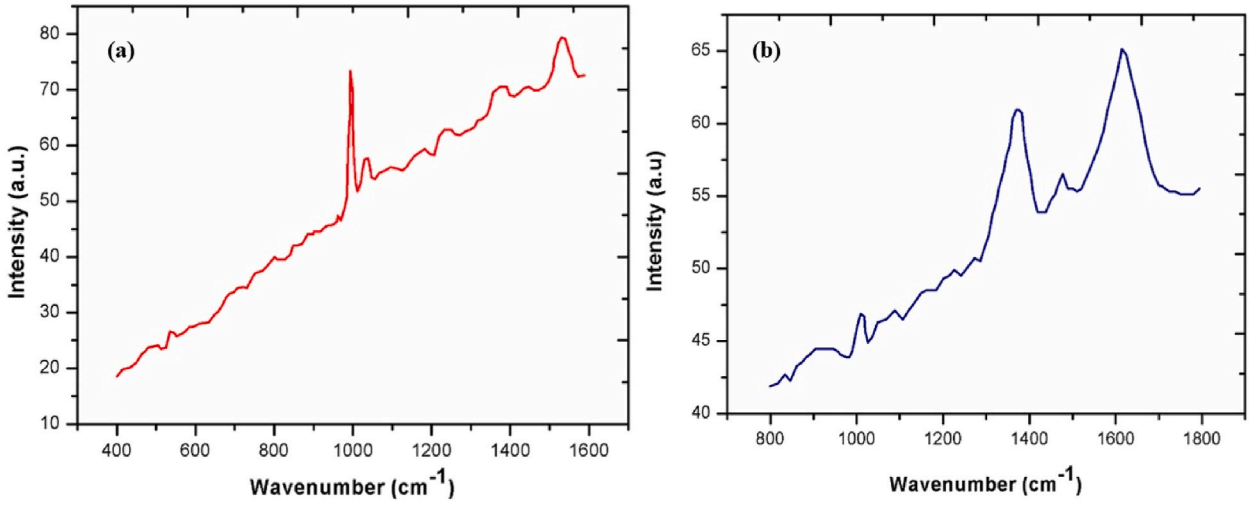

Fig. 9. Raman spectra of (a) nascent matrimid and (b) M@ MWCNT_10.

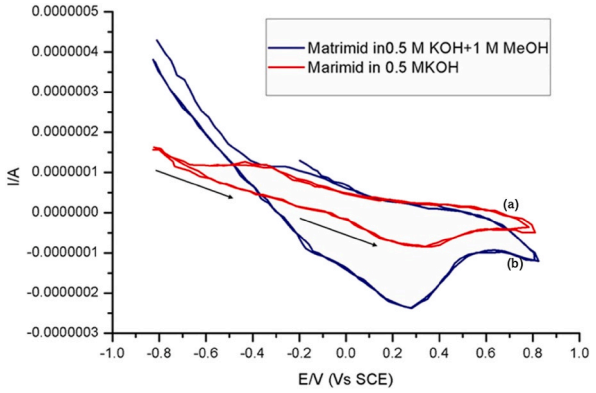

Fig. 10. Cyclic voltammogram of (a) matrimid and (b) stability curve of matrimid in 0.5 M KOH +1 M methanol with sweep rate of 50 mV s^{-1}.

3.10. Gas permeation analysis

The outcomes of testing the O_2/N_2 separation performance of all membranes employing constant-volume, differential pressure gas permeability studies are shown in Table 3.Quaternization of matrimid increased O_2/N_2 selectivity by 34 % while with O_2 permeability by 40.6 %. The O_2/N_2 selectivity went enhanced by 14.5–31.6% points when the *f*-MWCNT concentration was elevated from 5 to 10 wt %. This could be attributed to *f*-MWCNT agglomeration's previously reported barrier effect. In contrast, chloromethylation and quaternization of the Matrimid membrane increased O_2/N_2selectivity while decreasing O_2 permeability. The improvement in O_2/N_2selectivity was reported to be 6.9 % at 10 % quaternization of the Matrimid membrane, with a significant decrease in O_2 permeability (55.2 %). This is most likely due to a decrease in the fractional free volume of the quaternizedMatrimid due to intermolecular interactions, as seen in previous studies [52–55]. These findings show that modifying matrimid with functionalized MWCNT via chloromethylation and quaternization improves the interfacial morphology between the matrix (Matrimid) and the filler (*f*-MWCNT), lending performance-based support to the FESEM picture-based conclusion (Fig. 5).

f-MWCNTs, for instance, enhance gas separation performance by selectively diffusing one of the gas species (in this case, O_2) during

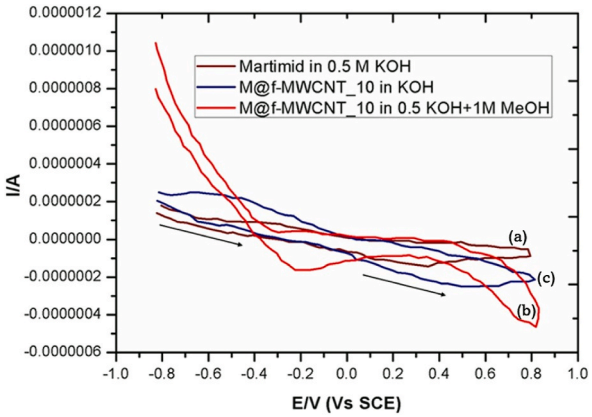

Fig. 11. (a) Comparative cyclic voltammogram of matrimid and M@*f*-MWCNT_10 in 0.5 M KOH, (b) 0.5 M KOH+1 M methanol and (c) stability curve of M@*f*-MWCNT_10 in 0.5 M KOH+1 M methanol with sweep rate of 50 mV s^{-1}.

Table 3
Gas permeability and selectivity of the membranes.

Membrane composition		O_2 Permeability (Barrer)	% Change (w.r.t.Matrimid)	O_2/N_2 Selectivity	% Change w.r.t.matrimid
Matrimid	*f*-MWCNT				
100	0	1.81 ± 0.32	–	5.89 ± 0.14	–
99.8	0.2	1.77 ± 0.17	−3.5	6.94 ± 1.6	24
99.6	0.4	2.87 ± 0.25	65.0	7.83 ± 1.39	34

the hopping process. When the carriers are free to move (as in a liquid medium), the transport event is typically simple, with the solute transported as "cargo." When the carrier is immobilised in a solid matrix (such as polymer-based separation membranes), the carriers must be distributed uniformly within the solid matrix for successful "hopping" events. As a result, it is critical to prevent carrier aggregation.

Taking into consideration the density of each membrane, a solubility-diffusivity study was carried out, as indicated in Table 4. All things considered, the solubility of oxygen and nitrogen is decreased when M@*f*-MWCNTs are added to the nascent Matrimid membrane. While the findings are provided in Tables 2 and it is clear that the inclusion of M@*f*-MWCNTs at a 5 wt % weight loading enhances solubility selectivity by 11.7 %. Significantly lower diffusivity selectivity was observed for the nanocomposite membranes (including M@*f*-MWCNT_10) compared to the pure matrimid membrane. There is peace and harmony between the parts when they are brought together to create a composite membrane. The strategy allowed us to overcome the obstacles of quaternizedMatrimid-*f*-MWCNT composite membranes, leading to significant enhancements in both O_2 diffusivity and O_2/N_2 selectivity.

Incorporation of fillers in gas separation membranes can influence both the solubility selectivity and the diffusivity selectivity of O_2/N_2 gas pairs. These variations are determined by the filler material's unique characteristics and its interaction with the membrane matrix. Here are some examples of generic effects: Solubility selectivity, adsorption sites, enhanced diffusion paths, surface modification, molecular sieving, hindered diffusion, and surface interaction are all examples of surface interactions. The effects of M@*f*-MWCNT incorporation on solubility selectivity and diffusivity selectivity are highly dependent on the specific filler material, its concentration, dispersion within the membrane matrix, and compatibility with the membrane material. These factors must be optimized in order to produce the necessary changes in gas separation performance.

4. Conclusions

The Matrimid membrane's O_2/N_2 separation performance was successfully improved using the modified multiwall carbon nanotube materials. The functionalized multiwall carbon nanotube performed as a functional carrier, which likely improved membrane homogeneity. When 10 wt% functionalized multiwall carbon nanotube is used for compatibilization, 5 wt% functionalized multiwall carbon nanotube enhanced both O_2 permeability (by 65 %) and O_2/N_2 selectivity (35 %), owing to 12.8 % and 37.2 % enhancement in O_2 diffusivity and O_2/N_2 selectivity, respectively. Thus, our findings show that changing carrier particles does not require a complicated method to improve performance in O_2/N_2 separation. Because of its viability, the projected technique is promising in creating membranes that could be beneficial in real-world applications.

Data availability statement

Data included in article/supp. Material/referenced in article.

Table 4
Solubility and diffusivity data for nascent Matrimid, M@*f*-MWCNT_5, and M@*f*-MWCNT_10 membranes.

Membrane	Density (g/cm^3)	O_2 Solubility (mol/m^3/bar)	N_2 Solubility (mol/m^3/bar)	O_2 Diffusivity (m^2/s) x10^{-12}	N_2 Diffusivity (m^2/s) x10^{-12}	O_2/N_2 Solubility selectivity	O_2/N_2 Diffusivity Selectivity
M@*f*-MWCNT_0	1.25	32.1	24.4	1.78	0.421	1.24	4.52
M@*f*-MWCNT_5	1.22	25.2	13.44	2.57	0.65	1.78	2.25
M@*f*-MWCNT_10	1.21	20.22	8.47	4.59	0.98	2.98	2.72

Additional information

No additional information is available for this paper.

CRediT authorship contribution statement

Mallikarjunagouda Patil: Conceptualization, Data curation. **Savitri G. Hunasikai:** Formal analysis. **Shridhar N. Mathad:** Formal analysis, Investigation. **Arun Y. Patil:** Formal analysis, Methodology, Writing – original draft. **Chandrashekhar G. Hegde:** Investigation, Methodology. **M.A. Sudeept:** Investigation, Methodology. **M.K. Amshumali:** Investigation. **Abdallah M. Elgorban:** Writing – original draft. **Shifa Wang:** Methodology. **Ling Shing Wong:** Software, Validation. **Asad Syed:** Conceptualization, Writing – original draft, Writing – review & editing.

Declaration of competing interest

Please check the following as appropriate.

- All authors have participated in (a) conception and design, or analysis and interpretation of the data; (b) drafting the article or revising it critically for important intellectual content; and (c) approval of the final version.
- This manuscript has not been submitted to, nor is under review at, another journal or other publishing venue.
- The authors have no affiliation with any organization with a direct or indirect financial interest in the subject matter discussed in the manuscript

Acknowledgments

The project was funded by the Vision Group for Science and Technology (VGST), Govt. Of Karnataka, Bengaluru, India, for a grant (GRD No. 951) (2020–2021) for establishing the laboratory at Basaveshwar Science College, Bagalkot, India. The author would like to express gratitude to VGST in Karnataka, India, for providing this opportunity. The authors extend their appreciation to the Deputyship for Research and Innovation, "Ministry of Education" in Saudi Arabia for funding this research (IFKSUOR3-299-5).

References

[1] A. Fernández-Barquín, C. Casado-Coterillo, S. Valencia, A. Irabien, Mixed matrix membranes for O_2/N_2 separation: the influence of temperature, Membranes 6 (2016) 28.
[2] D. Rana, T. Matsuura, Oxygen–nitrogen separation, in: Encyclopedia of Membrane Science and Technology, John Wiley & Sons, Inc., Hoboken, NJ, USA, 2013, pp. 1–26.
[3] K. Chong, S. Lai, H. Thiam, H. Teoh, S. Heng, Recent progress of oxygen/nitrogen separation using membrane technology, J. Eng. Sci. Technol. 11 (2016) 1016–1030.
[4] T.M. Stafford, Indoor air quality and academic performance, J. Environ. Econ. Manag. 70 (2015) 34–50.
[5] A.F. Ismail, Separation, in: E. Drioli, L. Giorno (Eds.), Encyclopedia of Membranes, Springer: Berlin/Heidelberg, Germany, 2016, pp. 1421–1422.
[6] H. Gong, C.Y. Chuah, Y. Yang, T.-H. Bae, High performance composite membranes comprising $Zn(pyrz)_2(SiF_6)$ nanocrystals for CO_2/CH_4 separation, J. Ind. Eng. Chem. 60 (2018) 279–285.
[7] C.Y. Chuah, W. Li, S. Samarasinghe, G. Sethunga, T.-H. Bae, Enhancing the CO2 separation performance of polymer membranes via the incorporation of amine-functionalized HKUST-1 nanocrystals, Microporous Mesoporous Mater. 290 (2019), 109680.
[8] G.M. Meyer, Method and apparatus for the production of nitrogen for use as an inert gas, U.S. Patent 3 (1975), 891,411, 24 June.
[9] A. Wellman, G. Stewart, Storage of brewing yeasts by liquid nitrogen refrigeration, Appl. Environ. Microbiol. 26 (1973) 577–583.
[10] D.E. Parfitt, A.A. Almehdi, Cryogenic storage of grape pollen, Am. Soc. Enol Viticulture 34 (1983) 227–228.
[11] C. Ordonez, M. Plummer, Cold thermal storage and cryogenic heat engines for energy storage applications, Energy Sources 19 (1997) 389–396.
[12] F.T. Bonner, Storage of seeds: potential and limitations for germplasm conservation, For. Ecol. Manag. 35 (1990) 35–43.
[13] A. Smith, J. Klosek, A review of air separation technologies and their integration with energy conversion processes, Fuel Process. Technol. 70 (2001) 115–134.
[14] C.Y. Chuah, K. Kim, J. Lee, D.-Y. Koh, T.-H. Bae, CO2 absorption using membrane contactors: recent progress and future perspective, Ind. Eng. Chem. Res. 59 (2020) 6773–6794.
[15] L.M. Robeson, Correlation of separation factor versus permeability for polymeric membranes, J. Membr. Sci. 62 (1991) 165–185.
[16] L.M. Robeson, The upper bound revisited, J. Membr. Sci. 320 (2008) 390–400.
[17] W. Li, K. Goh, C.Y. Chuah, T.-H. Bae, Mixed-matrix carbon molecular sieve membranes using hierarchical zeolite: a simple approach towards high CO2 permeability enhancements, J. Membr. Sci. 588 (2019), 117220.
[18] C.Y. Chuah, K. Goh, Y. Yang, H. Gong, W. Li, H.E. Karahan, M.D. Guiver, R. Wang, T.-H. Bae, Harnessing filler materials for enhancing biogas separation membranes, Chem. Rev. 118 (2018) 8655–8769.
[19] Y. Yang, C.Y. Chuah, L. Nie, T.-H. Bae, Enhancing the mechanical strength and $CO2/CH_4$ separation performance of polymeric membranes by incorporating amine-appended porous polymers, J. Membr. Sci. 569 (2019) 149–156.
[20] J.-R. Li, R.J. Kuppler, H.-C. Zhou, Selective gas adsorption and separation in metal–organic frameworks, Chem. Soc. Rev. 38 (2009) 1477–1504.
[21] V. Teplyakov, P. Meares, Correlation aspects of the selective gas permeabilities of polymeric materials and membranes, Gas Separ. Purif. 4 (1990) 66–74.
[22] C.Y. Chuah, T.-H. Bae, Incorporation of Cu_3BTC_2 nanocrystals to increase the permeability of polymeric membranes in $O2/N_2$ separation, BMC Chem. Eng. 1 (2019) 2.
[23] J. Adam, Z. Michael, M.H. David, B. Naomi, M. Ryan, C. Khetpakorn, A.R. Jeffrey, R.L. Jeffrey, Selective, High-Temperature O2 Adsorption in Chemically Reduced, Redox-Active Iron-Pyrazolate Metal–Organic Frameworks, ChemRxiv, 2019.
[24] L.J. Murray, M. Dinca, J. Yano, S. Chavan, S. Bordiga, C.M. Brown, J.R. Long, Highly-selective and reversible O2 binding in Cr_3(1,3,5-benzenetricarboxylate)$_2$, J. Am. Chem. Soc. 132 (2010) 7856–7857.
[25] Y. Li, R.T. Yang, Gas adsorption and storage in metal– organic framework MOF-177, Langmuir 23 (2007) 12937–12944.

[26] A. Fuoco, C. Rizzuto, E. Tocci, M. Monteleone, E. Esposito, P.M. Budd, M. Carta, B. Comesaña-Gándara, N.B. McKeown, J.C. Jansen, The origin of size-selective gas transport through polymers of intrinsic microporosity, J. Mater. Chem. A 7 (2019) 20121–20126.

[27] R. Kakuchi, P. Theato, Efficient multicomponent postpolymerization modification based on Kabachnik-Fields reaction, ACS Macro Lett. 3 (2014) 329–332.

[28] R. Swaidan, B. Ghanem, I. Pinnau, Fine-tuned intrinsically ultramicroporous polymers redefine the permeability/selectivity upper bounds of membrane-based air and hydrogen separations, ACS Macro Lett. 4 (2015) 947–951.

[29] M. Alberto, R. Bhavsar, J.M. Luque-Alled, A. Vijayaraghavan, P.M. Budd, P. Gorgojo, Impeded physical aging in PIM-1 membranes containing graphene-like fillers, J. Membr. Sci. 563 (2018) 513–520.

[30] P. Bernardo, F. Bazzarelli, F. Tasselli, G. Clarizia, C.R. Mason, L. Maynard-Atem, P.M. Budd, M. Lanč, K. Pilnáček, O. Vopička, et al., Effect of physical aging on the gas transport and sorption in PIM-1 membranes, Polymer 113 (2017) 283–294.

[31] R. Hou, S.J.D. Smith, C.D. Wood, R.J. Mulder, C.H. Lau, H. Wang, M.R. Hill, Solvation effects on the permeation and aging performance of PIM-1-based MMMs for gas separation, ACS Appl. Mater. Interfaces 11 (2019) 6502–6511.

[32] S. Harms, K. Rätzke, F. Faupel, N. Chaukura, P.M. Budd, W. Egger, L. Ravelli, Aging and free volume in a polymer of intrinsic microporosity (PIM-1), J. Adhesion 88 (2012) 608–619.

[33] H. Nagar, P. Vadthya, N.S. Prasad, S. Sridhar, Air separation by facilitated transport of oxygen through a Pebax membrane incorporated with a cobalt complex, RSC Adv. 5 (2015) 76190–76201.

[34] N. Preethi, H. Shinohara, H. Nishide, Reversible oxygen-binding and facilitated oxygen transport in membranes of polyvinylimidazole complexed with cobalt-phthalocyanine, React. Funct. Polym. 66 (2006) 851–855.

[35] H. Li, W. Choi, P.G. Ingole, H.K. Lee, I.H. Baek, Oxygen separation membrane based on facilitated transport using cobalt tetraphenylporphyrin-coated hollow fiber composites, Fuel 185 (2016) 133–141.

[36] Q. Zheng, S.J. Thompson, S. Zhou, M. Lail, K. Amato, A.V. Rayer, J. Mecham, P. Mobley, J. Shen, B. Fletcher, Task-specific ionic liquids functionalized by Cobalt (II) salen for room temperature biomimetic dioxygen binding, Ind. Eng. Chem. Res. 58 (2018) 334–341.

[37] S. Samarasinghe, C.Y. Chuah, W. Li, G. Sethunga, R. Wang, T.-H. Bae, Incorporation of Co^{III} acetylacetonate and SNW-1 nanoparticles to tailor $O2/N_2$ separation performance of mixed-matrix membrane, Sep. Purif. Technol. 223 (2019) 133–141.

[38] M.O. Midda, A.K. Suresh, Some mechanistic insights into the action of facilitating agents on gas permeation through glassy polymeric membranes, AIChE J. 64 (2018) 186–199.

[39] M. Rezakazemi, A.E. Amooghin, M.M. Montazer-Rahmati, A.F. Ismail, T. Matsuura, State-of-the-art membrane based CO_2 separation using mixed matrix membranes (MMMs): an overview on current status and future directions, Prog. Polym. Sci. 39 (2014) 817–861.

[40] A. Emplit, F.F. Tao, P. Lipnik, G. Heunen, C. Bailly, I. Huynen, Polypropylene carbon nanotubes nanocomposites: combined influence of block copolymer compatibilizer and melt annealing on electrical properties, J. Nanomater. 2017 (2017).

[41] R. Patel, J.T. Park, H.P. Hong, J.H. Kim, B.R. Min, Use of block copolymer as compatibilizer in polyimide/zeolite composite membranes, Polym. Advan. Technol. 22 (2011) 768–772.

[42] Mallikarjunagouda B. Patil, Shwetarani B. Rajamani, S.N. Mathad, Y. Arun, Patil Mahmoud, A. Hussain, Hajer Saeed Alorfii, Anish Khan, Abdullah M. Asiri, Imran Khan, Madhu Puttegowda, Microwave-assisted synthesis of poly (acrylamide-co-2-hydroxyethyl methacrylate)/chitosan semi-IPN ZnO nanocomposite membranes for food packaging applications, J. Mater. Res. Technol. 20 (2022) 3537–3548, https://doi.org/10.1016/j.jmrt.2022.08.079.

[43] A.A. Otaibi, M.B. Patil, S.B. Rajamani, S.N. Mathad, A.Y. Patil, M.K. Amshumali, J.P. Shaik, A.M. Asiri, A. Khan, Development and testing of zinc oxide embedded sulfonated poly (vinyl alcohol) nanocomposite membranes for fuel cells, Crystals 12 (2022) 1739, 10.3390/cryst12121739.

[44] A.F. Bushell, P.M. Budd, M.P. Attfield, J.T.A. Jones, T. Hasell, A.I. Cooper, P. Bernardo, F. Bazzarelli, G. Clarizia, J.C. Jansen, Nanoporous organic polymer/cage composite membranes, Angew. Chem. Int. Ed. 52 (2013) 1253–1256.

[45] M.B. Patil, S.N. Mathad, A.Y. Patil, A. Khan, M.A. Hussein, A.M. Alosaimi, A.M. Asiri, A. Manikandan, M.M.A. Khan, Functional properties of grapefruit seed extract embedded blend membranes of poly(vinyl alcohol)/starch: potential application for antiviral activity in food safety to fight against COVID-19, J. Polym. Environ. 31 (6) (2023) 2519–2533, https://doi.org/10.1007/s10924-022-02742-5.

[46] S. Samarasinghe, C.Y. Chuah, Y. Yang, T.-H. Bae, Tailoring CO_2/CH_4 separation properties of mixed-matrix membranes via combined use of two-and three-dimensional metal-organic frameworks, J. Membr. Sci. 557 (2018) 30–37.

[47] W. Li, C.Y. Chuah, L. Nie, T.-H. Bae, Enhanced $CO2/CH_4$ selectivity and mechanical strength of mixed-matrix membrane incorporated with NiDOBDC/GO composite, J. Ind. Eng. Chem. 74 (2019) 118–125.

[48] T. Al Kayal, D. Panetta, B. Canciani, P. Losi, M. Tripodi, S. Burchielli, P. Ottoni, P.A. Salvadori, G. Soldani, Evaluation of the effect of a gamma irradiated DBM-pluronic F127 composite on bone regeneration in Wistar rat, PLoS One 10 (2015), e0125110.

[49] X. Yin, L.S. Daintree, S. Ding, D.M. Ledger, B. Wang, W. Zhao, J. Qi, W. Wu, Itraconazole solid dispersion prepared by a supercritical fluid technique: preparation, in vitro characterization, and bioavailability in beagle dogs, Drug Des. Devel. Ther. 9 (2015) 2801.

[50] X. Ji, T. Zou, H. Gong, Q. Wu, Z. Qiao, W. Wu, H. Wang, Cobalt phthalocyanine nanowires: growth, crystal structure, and optical properties, Crys. Res. Technol. 51 (2016) 154–159.

[51] B. Karolewicz, A. Górniak, A. Owczarek, E. Żurawska-Płaksej, A. Piwowar, J. Pluta, Thermal, spectroscopic, and dissolution studies of ketoconazole–Pluronic F127 system, J. Therm. Anal. Calorim. 115 (2014) 2487–2493.

[52] C.Y. Chuah, Y. Yang, T.-H. Bae, Hierarchically porous polymers containing triphenylamine for enhanced SF_6 separation, Microporous Mesoporous Mater. 272 (2018) 232–240.

[53] M. Thommes, K. Kaneko, A.V. Neimark, J.P. Olivier, F. Rodriguez-Reinoso, J. Rouquerol, K.S. Sing, Physisorption of gases, with special reference to the evaluation of surface area and pore size distribution (IUPAC Technical Report), Pure Appl. Chem. 87 (2015) 1051–1069.

[54] X. Wu, Z. Tian, S. Wang, D. Peng, L. Yang, Y. Wu, Q. Xin, H. Wu, Z. Jiang, Mixed matrix membranes comprising polymers of intrinsic microporosity and covalent organic framework for gas separation, J. Membr. Sci. 528 (2017) 273–283.

[55] Q. Zhou, L. Zhang, M. Zhang, B. Wang, S. Wang, Miscibility, free volume behavior and properties of blends from cellulose acetate and castor oil-based polyurethane, Polymer 44 (2003) 1733–1739.